

# Twist-averaged Boundary Conditions in Continuum Quantum Monte Carlo

C. Lin, F.-H. Zong and D. M. Ceperley

*Dept. of Physics and NCSA, University of Illinois at Urbana-Champaign, Urbana, IL 61801*

We develop and test Quantum Monte Carlo algorithms which use a “twist” or a phase in the wave function for fermions in periodic boundary conditions. For metallic systems, averaging over the twist results in faster convergence to the thermodynamic limit than periodic boundary conditions for properties involving the kinetic energy with the same computational complexity. We determine exponents for the rate of convergence to the thermodynamic limit for the components of the energy of coulomb systems. We show results with twist averaged variational Monte Carlo on free particles, the Stoner model and the electron gas using Hartree-Fock, Slater-Jastrow, three-body and backflow wavefunction. We also discuss the use of twist averaging in the grand canonical ensemble, and numerical methods to accomplish the twist averaging.

PACS Numbers: 02.70.-c, 82.20.Wt, 71.15.-m

Almost all quantum Monte Carlo (QMC) calculations in periodic boundary conditions have assumed that phase of the wavefunction returns to the same value if a particle goes around the periodic boundaries and returns to its original position. However, with these boundary conditions, delocalized fermion systems converge slowly to the thermodynamic limit because of shell effects in the filling of single particle states. In this paper we explore an alternative boundary condition: one can allow particles to pick up a phase when they wrap around the periodic boundaries,

$$\Psi(\mathbf{r}_1 + L\hat{x}, \mathbf{r}_2, \dots) = e^{i\theta_x} \Psi(\mathbf{r}_1, \mathbf{r}_2, \dots). \quad (1)$$

The boundary condition  $\theta = 0$  is called periodic boundary conditions (PBC),  $\theta = \pi$  anti-periodic boundary conditions (ABC) and the general condition with  $\theta \neq 0$ , twisted boundary conditions (TBC)<sup>1</sup>.

In periodic boundary conditions, the Hamiltonian is invariant with respect to translating any particle around the periodic boundaries. According to Bloch’s theorem, this implies that any solution can be characterized by a given twist angle. The twist angle also has a physical origin: consider a toroidal geometry. One can either rotate the torus<sup>2</sup> and go into rotating coordinates, or add a magnetic flux<sup>3</sup> to the center of the torus. The physical properties will be unchanged. In both cases one can transform away the perturbation by applying TBC with the twist angle given by  $\theta = mR^2\omega/h$  for rotation and  $\theta = e\phi/(c\hbar)$  for magnetic flux. A torus is topologically equivalent to periodic boundary conditions, so that a non-zero twist will be allowed in periodic boundaries. The twist is a degree of freedom, or boundary condition, that can be varied to enable a finite system to approach the thermodynamic limit more quickly or to make detailed studies of the properties of the quantum state.

If the periodic boundaries are used in all three directions, each dimension can have an independent twist<sup>4</sup>. Hence, in 3D, the twist is a three component vector,  $\theta_i$  with  $i = \{1, 2, 3\}$ . The free energy and hence all equilibrium properties are (triply) periodic<sup>3</sup> in the twist:  $F(\theta_i + 2\pi) = F(\theta_i)$  so that each component of the twist

can be restricted to be in the range:

$$-\pi < \theta_i \leq \pi. \quad (2)$$

For systems with a real potential (*e.g.* no magnetic field), one can further restrict the twist to be in the range  $[0, \pi]$ .

For a degenerate Fermi liquid, finite-size shell effects are much reduced if the twist angle is averaged over. We call this twist averaged boundary conditions (TABC)<sup>5</sup>. This is particularly important in computing properties that are sensitive to the single particle energies such as the kinetic energy and the magnetic susceptibility. By reducing shell effects, much more accurate estimations of the thermodynamic limit of these properties can be made. What makes this even more important is that the most accurate quantum methods have computational demands which increase rapidly with the number of fermions. Examples of such methods are exact diagonalization<sup>6</sup> (exponential increase in CPU time with  $N$ ), variational Monte Carlo<sup>7</sup> (VMC) with wavefunctions having backflow and three-body terms<sup>8,9</sup> (increases as  $N^4$ ), and transient-estimate and released-node Diffusion Monte Carlo methods<sup>10</sup> (exponential increase with  $N$ ). Methods which can extrapolate more rapidly to the thermodynamic limit are crucial in obtaining high accuracy. Twist averaging is especially advantageous for stochastic methods (*i.e.* QMC) because the averaging does not necessarily slow down the evaluation of averages, except for the necessity of doing complex rather than real arithmetic.

The use of twisted boundary conditions is commonplace for the solution of the band structure problem for a periodic solid. Band structure methods begin by assuming the wavefunction factors into single particle orbitals characterized by a lattice momentum. Then in order to calculate properties of an infinite periodic solid, properties must be averaged by integrating over the first Brillouin zone. Baldereschi<sup>11</sup> pointed out that in an insulator, in integrating over the Brillouin zone, one can with high accuracy replace the integral with a “special k-point.” This was generalized to a grid of k-points<sup>12</sup>.

Twisted boundary conditions has been discussed in connection with polarization of insulators<sup>13</sup>; we do not consider that here. The use of twisted boundary conditions is common in the analysis of lattice models<sup>6,14</sup>. Gammel<sup>15</sup> showed using perturbation arguments for certain lattice models why it will converge faster to the thermodynamic limit and applied it to calculating optical properties. Gros<sup>16</sup> studied size effects in the Hubbard model with exact diagonalization and showed TABC gives exact results in the grand canonical ensemble for non-interacting systems.

Though twisted boundary conditions have a long history within quantum physics, their use in quantum Monte Carlo (QMC) has been limited. In continuum QMC, Rajagopal<sup>17</sup> used special k-points to reduce finite size errors for calculations of insulators within VMC. Their use in Diffusion Monte Carlo (DMC) results were restricted to PBC and ABC in order to work with real wavefunctions. Kralik *et al.*<sup>18</sup> used generalized boundary conditions to compute the momentum distribution with VMC for silicon (a semiconductor) and Filippi and Ceperley<sup>19</sup> for lithium (a metal). This was done in order to enlarge the number of momentum vectors to probe the behavior near the fermi surface. The use of TABC within QMC has not been further developed.

The applications considered here are for systems with a fermi surface, *i.e.* metals. We begin by discussing the method for non-interacting (NI) fermions. Fermi liquid theory asserts that the spectrum of states of interacting liquids are intimately related to those of the non-interacting fermion systems, hence a detailed analysis for the NI system carries over to strongly interacting fermi liquids. We then discuss interacting systems in the Hartree-Fock approximation: the electron gas and the Stoner model. In the Stoner model, we show how TABC can be used to determine a polarization phase transition at non-zero temperature. Results for TABC are given for the interacting electron gas using a pair product and backflow wavefunction in 3d. The electron gas system has been previously treated with an extrapolation method based on Fermi liquid theory. We show that TABC gives the same results in the thermodynamic limit and verify the applicability of the NI analysis, in particular to examine how the energy depends on the twist of a given system size. We then present VMC results of the polarization energy of the electron gas using the new method. In future publications we will study the low density properties of the electron gas using this technique. The Appendix discusses some details arising in the implementation of TABC in QMC.

## I. NON-INTERACTING FERMIONS

In a non-interacting homogenous system with PBC, the single particle states are plane waves:  $\exp(i\mathbf{k}\mathbf{r})\eta(\sigma)$  where  $\eta$  is a spin function. For simplicity, we always as-

sume the simulation cell is a cube (or square in 2D) of side  $L$ . To satisfy the twisted boundary conditions, the wave vectors obey:

$$\mathbf{k}_{\mathbf{n}} = (2\pi\mathbf{n} + \theta)/L \quad (3)$$

where  $\mathbf{n}$  is an integer vector. These states have energy  $E_{\mathbf{n}} = (\hbar^2/2m)\mathbf{k}_{\mathbf{n}}^2$ . The ground state in the canonical ensemble consists of the  $N$  lowest energy states; the many-body wavefunction is a determinant of those states. In this section we will ignore spin, since for a non-interacting system, spin modifies the results only by doubling the degeneracy of each level. Figure 1 shows the occupation of states for 13 spin-less fermions in 2D for  $\theta = 0$  *i. e.* with periodic boundary conditions, and also with a non-zero twist. The occupied states lie within a circle centered at the origin with radius  $\approx k_F = 2(\pi\rho)^{1/2}$ .

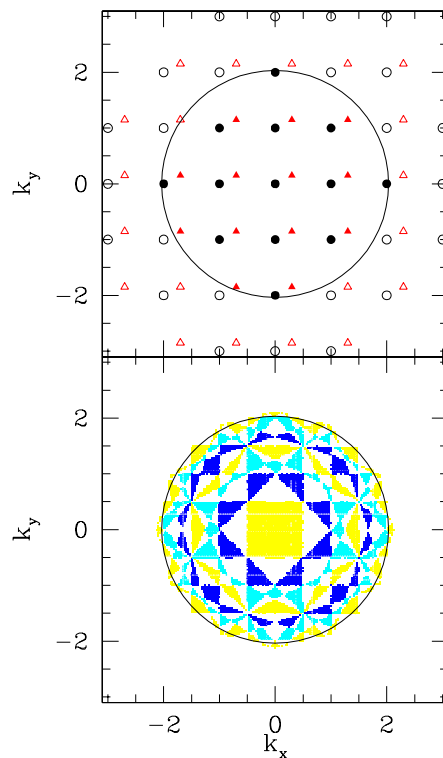


FIG. 1. Momentum distribution for 13 spinless fermions in a 2D square with side  $L = 2\pi$ . The top panel shows the occupied states (closed symbols) and empty states (open symbols) with zero twist (circles, PBC) and a twist equal to  $2\pi(0.3, 0.15)$  (triangles). The circle shows the infinite system fermi surface. The bottom panel shows the occupied states with TABC. The colored regions show the occupied region for the lowest level (middle square), the third level, up to the outermost 13<sup>th</sup> level.

Figure 2 shows the relative error in energy versus the number of fermions with PBC. The energy converges slowly to the exact result. One sees “cusps” in the curve at certain values of  $N$ . These occur at closed-shell values of  $N$ , *e.g.* the state depicted in Fig. 1 for PBC is a closed shell since states related by symmetry are either all filled

or all empty. For large  $N$  the curve is “quasi-random”, with an envelope decaying algebraically as  $N^{-\nu}$ .

We find numerically that the exponent of the decay of the relative error of the energy is approximately  $\nu = 1.33$  in 2D and  $\nu = 1$  in 3D (see Table I). To characterize the approach to the thermodynamic limit, we introduce two different measures. Defining the relative scaled error  $\delta_N$  as:

$$E_N = E_\infty(1 + N^{-\nu}\delta_N), \quad (4)$$

we define  $a = \max|\delta_N|$ ,  $b = \langle\delta_N\rangle$  and  $c = \langle(\delta_N - b)^2\rangle^{1/2}$ . Table I shows estimates of these coefficients and exponents obtained numerically by examining values of  $10 \leq N \leq 10^4$ .

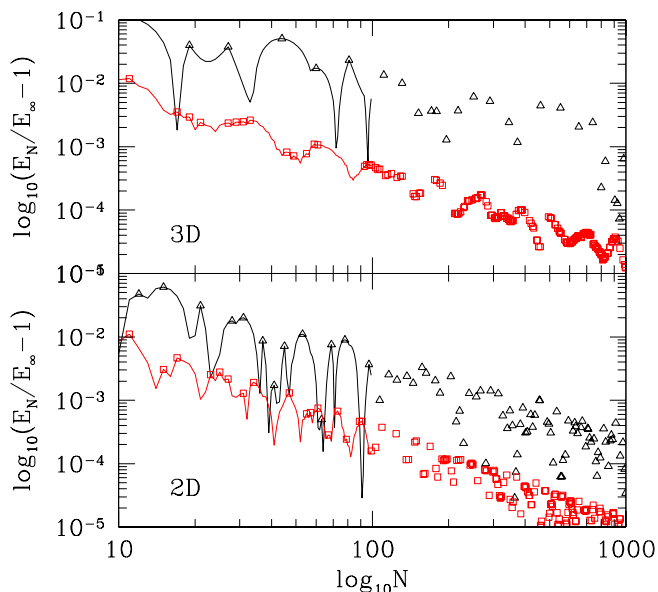


FIG. 2. Relative error of the energy versus number of particles with PBC ( $\triangle$ ) and TABC ( $\square$ ) in 2D and 3D. The points shown are only those where the relative error has a local maximum. Curves are shown only for  $N < 100$ .

Now consider twisting the boundary conditions, *i. e.* using a nonzero phase. This displaces the set of  $\mathbf{k}$ -vectors as shown in the top panel of Fig. 1. Aside from a set of special twists having zero measure, the energy levels will no longer be degenerate. (When we sort the states to decide the filling, all states will have a different energy.) This is because inversion symmetry and rotational symmetry through  $90^\circ$  is broken. This breaking of symmetries and absence of degeneracies is a crucial difference between TBC and PBC.

At critical values of the twist, when a filled and empty state have the same energy, the occupation of the states changes. The condition for the degeneracy is that  $\mathbf{k}$  lie

on a plane bisecting and perpendicular to the line joining the origin with an integer vector; precisely the Laue condition for the Bragg planes<sup>20</sup> of the reciprocal lattice of the supercell. In fig. 3 is shown the dependence of total energy on the twist angle for a fixed number of particles. One sees cusps as the filled states cross the Bragg planes. The dependence is similar to the band energy of a simple metal. Later, we will discuss this band structure for an interacting system. The bandwidth  $E_{BW}$  (the spread of energy values fig. 3) is defined as:

$$E_{BW}^2 = (2\pi)^{-d} \int d\theta (E(\theta) - E_\infty)^2 \quad (5)$$

depends on the number of particles and scales as  $E_{BW} \propto N^{-\nu}$  where the exponent is the same as describes the convergence of the KE in PBC.

There are several alternative procedures by which the twist angle can be varied: i) one can average the twist over all possible values, ii) the twist can become a dynamical variable and iii) special values of the twist could be used. Of these approaches, none are right or wrong in general; which method approaches the thermodynamic limit faster depends on the order of the phase in question, whether fermi liquid, ferromagnetic or anti-ferromagnetic. However, to compute a variety of properties for a metallic systems, we find the TABC best reduces size effects.

n	O	d	$\nu$	a	b	c
1	T	2	1.33	4.5	0.37	1.77
8	T	2	1.5	0.47	0.27	0.093
1	N	2	0.67	2.18	0	0.65
16	N	2	0.75	0.71	0	0.52
1	V	2	1	0.50	-0.35	0.069
8	V	2	1	0.38	-0.367	0.0058
1	T	3	1	2.4	0.25	1.0
8	T	3	1.33	0.50	0.292	0.065
16	T	3	1.33	0.35	0.21	0.06
32	T	3	1.33	0.35	0.19	0.06
1	N	3	0.55	2.97	0	1.00
16	N	3	0.67	0.83	0	0.63
1	V	3	0.67	0.742	-0.549	0.072
16	V	3	0.67	0.587	-0.582	0.0043

TABLE I. Coefficients of the asymptotic decay of the error in the relative NI energy.  $\nu$  is the exponent of the decay. The exponents have been determined from the numerical data and are accurate to about 0.02. The amplitude was determined numerically by examining the values for  $10 \leq N \leq 10000$ . The coefficients are defined as  $a \equiv \max(|\delta_N|)$ ,  $b = \langle\delta_N\rangle$ ,  $c = \langle[\delta_N - b]^2\rangle^{1/2}$ .  $n$  is the number of phase angles used for the summation in each dimension:  $\theta_i = 2\pi i/n$  for  $i = 1, \dots, n$ .  $n = 1$  corresponds to PBC;  $d$  is the dimensionality.  $O$  is the property:  $T$ , the kinetic energy;  $V$ , the Hartree-Fock potential energy of the electron gas;  $N$ , the number of particles in the TA-GCE method.

## II. TWIST AVERAGING

The twist average of a property  $\hat{A}$  is defined by:

$$\langle \hat{A} \rangle = (2\pi)^{-d} \int_{-\pi}^{\pi} d\theta \langle \psi(R, \theta) | \hat{A} | \psi(R, \theta) \rangle \quad (6)$$

where it is assumed that the wavefunction  $\psi(R, \theta)$  is normalized for each  $\theta$ . The momentum distribution,  $n(\mathbf{k})$  is a key property to calculate for delocalized quantum systems. A discontinuity in  $n(\mathbf{k})$  at the Fermi surface is responsible for the validity of Fermi Liquid Theory for metals. The kinetic energy is the second moment of the momentum distribution:

$$T_N = (\hbar^2/2m) \int d\mathbf{k} k^2 n(\mathbf{k}). \quad (7)$$

Let us analyze the momentum distribution for NI fermions in the canonical ensemble. For any given twist  $\theta$ , the  $N$  lowest energy states from those given by Eq. 3 are occupied. But any value of  $\mathbf{k}$  can only be reached by a unique combination of  $(\mathbf{n}, \theta)$  if  $\theta$  is restricted by Eq. 2. This proves that the averaged momentum distribution is a constant for states which can be reached by some combination of  $(\mathbf{n}, \theta)$  and zero otherwise. Hence within TABC, the set of filled states comprises a “solid volume” bounded by a Fermi surface. In contrast, for a single twist value, the momentum distribution is a point set. The total volume in  $k$ -space inside the Fermi surface is precisely  $(2\pi)^d \rho$ , just as it is in the thermodynamic limit, so the constant is determined by the normalization condition:

$$\int d\mathbf{k} n(\mathbf{k}) = 1. \quad (8)$$

As mentioned above, the Fermi surface is a subset of the Bragg planes. For  $N$  particles the occupied states comprise the union of the first  $N$  Brillouin zones<sup>20</sup>. The  $(N+1)^{th}$  electron will go in the  $(N+1)^{th}$  zone, an area formed by planes surrounding the  $N^{th}$  zone. Figure 1 shows the momentum distribution of 13 spinless fermions in 2D using TABC.

In 1D, TABC gives the exact momentum distribution because the normalization condition determines everything. In higher dimensions the Fermi surface is not perfectly circular (spherical) as shown in fig. 1. However, one can see that  $n(\mathbf{k})$  is much closer to a disk than the momentum distribution obtained with PBC. A perfect Fermi surface (no finite size corrections) in any dimension, can be obtained by allowing variations in the particle number and working in the grand canonical ensemble as we discuss below.

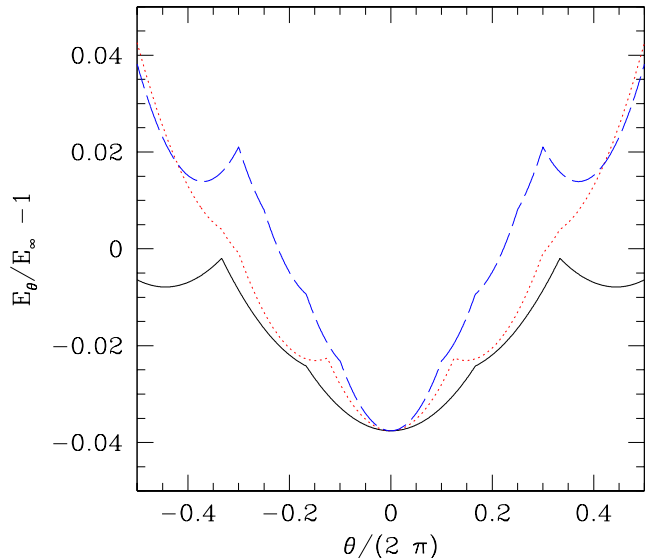


FIG. 3. Dependence of the energy of NI unpolarized fermions on the twist angle for  $N=54$  in 3D. The solid line shows the energy along the (100) direction, dotted line along the (110) direction and dashed line along the (111) direction. The curves are piecewise quadratic, with a cusp when the occupation of the states changes. We refer to the r.m.s. spread of energy values as the bandwidth.

Figure 2 shows the convergence of the error of the kinetic energy within TABC versus the number of particles. Numerical estimates of the relative error are given in Table I. One sees a dramatic improvement in the convergence with respect to PBC. The exponents governing the decay rate are larger and the errors are up to two orders of magnitude smaller for system sizes in the range  $N \approx 100$ . Note that the TABC kinetic energy must approach the exact energy from above. This is because the shape of a given volume with the smallest moment of inertia is a sphere, so that the distorted shape shown in fig. 1 has a higher energy. Also shown in Table I is dependence of the error on the number of twist values in the average. One needs from 16 to 32 values of  $\theta$  along each axis to achieve the full reduction in size effects (better than a percent accuracy in the relative error of the size effects). In the Appendix are discussed the relative merits of performing the average on a grid versus sampling the twist values from a uniform distribution.

Let us now examine how the potential energy converges with PBC and TABC. This will give us some idea of how two particle correlations are affected by the boundary conditions since the potential energy is a particular integral over the pair correlation function. The calculation performed below is particularly simple for a power law

potential,  $v(r) = r^{-n}$ . In particular, we examine the potential energy of an electron gas ( $n = 1$ ) computed using the NI wavefunction (Hartree-Fock approximation). The NI trial function is valid for high density when the kinetic energy dominates the potential energy. The potential energy (using the Ewald image potential) is conveniently evaluated in Fourier space as a sum over the structure factor:

$$V = \frac{N\rho}{2} \sum_{\mathbf{k}} v_{\mathbf{k}}(S_{\mathbf{k}} - 1) + Nv_M \quad (9)$$

where  $v_M$  is the Madelung energy of a charge interacting with itself and  $v_{\mathbf{k}}$  is the Fourier transform of the interparticle potential. For a  $1/r$  potential,  $v_k = 2\pi(d-1)/k^{d-1}$ . The values of  $\mathbf{k}$  in the sum are  $\mathbf{k} = 2\pi\mathbf{n}/L$  where  $\mathbf{n}$  is an integer vector. For the NI wavefunction, the structure factor at wave-vector  $\mathbf{q}$  is proportional to the probability that after we have displaced a filled state by  $\mathbf{q}$  we are still in a filled state.

$$S_{\mathbf{q}} = 1 - \frac{1}{N} \left\langle \sum_{\mathbf{k} < \mathbf{k}'} \delta(\mathbf{k} - \mathbf{k}' - \mathbf{q}) \right\rangle \quad (10)$$

where the sum is over occupied states and the average is over twisted boundary conditions.

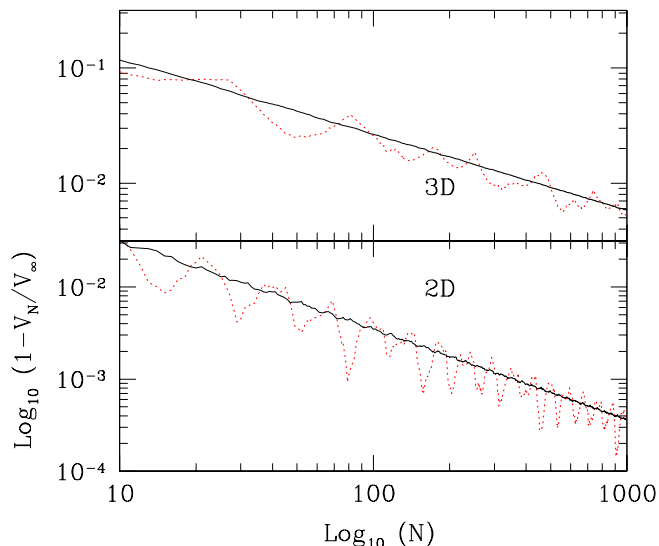


FIG. 4. Relative error in the evaluation of the potential energy for an electron gas using the Hartree-Fock wavefunction for  $N$  spinless electrons. The solid line shows TABC, the dashed line PBC.

Shown in fig. 4 is the convergence of the potential energy versus the number of particles using PBC and

TABC. For all values of  $N$  and twists the potential energy of the finite systems approaches that of the infinite systems from below. Twist averaging serves to make the decay more regular but does not reduce its overall magnitude which is determined by a charge interacting with the correlation hole in the nearby supercell. Similar effects are expected for other two particle quantities. The smoother convergence obtained with TABC should allow for more accurate extrapolation to  $N \rightarrow \infty$ .

### III. GRAND CANONICAL ENSEMBLE

The use of TABC in the grand canonical ensemble (GCE) gives the exact single particle occupations for NI particles, as shown by Gros<sup>16</sup> within the Hubbard model. Suppose  $(\alpha, N)$  is a label of the quantum states, both for the number of particles and for other quantum numbers such as the momentum and let  $E_{\alpha, N}(\theta)$  be the energy of this state. Then the probability of a given state in the GCE is proportional to  $\exp(-\beta(E_{\alpha, N}(\theta) - N\mu))$  where  $\mu$  is the chemical potential. In the ground state,  $\beta \rightarrow \infty$ , the occupied many-body state will be the one minimizing  $E_{\alpha, N}(\theta) - N\mu$ . Thus  $N$  can depend on  $\theta$ .

We now show that for a NI system, TABC within the GCE gives exact single particle properties; *i.e.* there are no finite size effects. Suppose the single particle energy levels are  $e_k$ . Then the probability of occupying the  $N$  states  $e_1, \dots, e_n$  is  $\exp(-\sum_{k=1}^N \beta[e_k(\theta) - \mu])$ . In the occupation number  $\hat{n}_k$  basis, this probability distribution factorizes as:

$$\prod_{\mathbf{k}} \left[ \hat{n}_k e^{-\beta[e_k(\theta) - \mu]} + (1 - \hat{n}_k) \right] \quad (11)$$

so the probability of state  $k$  being occupied is precisely the fermi distribution law  $n_k = (\exp(\beta(e_k - \mu)) + 1)^{-1}$ . As the twist angle is varied over its range, each momentum state of the infinite system occurs precisely once. Hence the averaged occupation number is precisely what it would be in the thermodynamic limit. The distortion of the fermi surfaces observed in the lower panel of fig. 1 is a consequence of using the canonical ensemble.

The momentum distribution and hence the kinetic energy will be exactly equal to their infinite system values. Other properties may have finite size corrections, only the single particle properties are guaranteed to be exact. We call this procedure the twist average grand canonical ensemble (TA-GCE).

With this procedure one does not have a fixed number of particles since for a given twist and fermi wave vector, the number of occupied states will vary. The fluctuations in the number of particles is closely related to a famous problem in analytic number theory, ‘‘Gauss’ circle problem’’, to determine the number of lattice points inside a circle of area  $A$  as its radius tends to infinity<sup>21</sup>. As Gauss posed the problem, the center of the circle was fixed on

a lattice site while in TA-GCE the circle is placed randomly (the shifted circle problem). It has been shown<sup>22</sup> that in 2D one obtains the following fluctuation in the particle number for TA-GCE:

$$\lim_{N \rightarrow \infty} \langle (N - (Lk_F)^2/4\pi)^2 \rangle^{1/2} \propto N^{1/4}. \quad (12)$$

Our numerical estimates for the convergence are shown in Table I. Note that the Gauss circle problem differs from the convergence of the energy in the canonical ensemble since the energy is the average second moment of the lowest  $N$  points, not the number of points in a circle.

The preceding discussion refers to NI systems, however, fermi liquid theory asserts that the low lying excited states of an interacting system are in one-to-one correspondence with the NI states. Hence, as argued by Gross<sup>16</sup> and Gammel<sup>15</sup>, TA-GCE is likely to reduce finite size effects substantially for interacting systems.

For an interacting many-body system, one difficulty in using the GCE is the need to optimize the wavefunction at each twist value; in particular to pick out which orbitals should be occupied. For an isotropic system having a spherical fermi surface, the order of filling the states is simple. For a metal with a non-spherical Fermi surface, the usual procedure is to determine the filling of single particle states according to a mean-field theory such as the Kohn-Sham method in density functional theory. If one uses the same procedure within QMC, the Fermi surface will be substantially unchanged. Hence, it would be better to try other fillings, choosing the one which minimizes  $E_N - N\mu$ .

There are other problems in using the GCE for charged systems in periodic boundary conditions. Usually the positive compensating charge, either a uniform background or a fixed array of charged nuclei, is at a fixed density. But if the number of electrons fluctuates, the periodic cell can have a net charge, which causes problems in calculating the long-range potential. Although very promising, we do not consider the TA-GCE method further in this paper. The following examples are for the canonical ensemble.

#### IV. THE STONER MODEL

To test the utility of TABC for determining a phase transition, we simulated the Stoner model, an analytically solvable model<sup>23,24</sup> for strongly correlated fermions, particularly related to itinerant magnetism<sup>25</sup>. The Stoner model differs from NI fermions by the addition of a contact repulsive potential:  $\sum_{i < j} g\delta(r_{ij})$ . The energy is evaluated within the mean field (Hartree-Fock) approximation using the NI wavefunction. For a spin (1/2) system, the potential energy is  $E = E_{NI} + gn_{\uparrow}n_{\downarrow}$ . In 3D the energy at zero temperature in the thermodynamic limit is:

$$E/N = \lambda \frac{(3\pi^2\rho)^{5/3}}{10\pi^2} [(1 + \zeta)^{5/3} + (1 - \zeta)^{5/3} + b(1 - \zeta^2)] \quad (13)$$

where  $b = \frac{5g\rho}{6\lambda}(3\pi^2\rho)^{-2/3}$  and  $\lambda = \hbar^2/2m$ . For  $b < 1.111$  the system has an unpolarized ground state and for  $b > 1.3228$  the ground state is ferromagnetic. For intermediate couplings, the ground state has a partial spin polarization at zero temperature, similar to the behavior suggested<sup>26,27</sup> for the electron gas at low density.

We performed a MC simulation of the 3D NI system, within the occupation representation. The state variables of the system consist of occupation numbers (both spin and wavevector) and the twist angles. We make Monte Carlo moves consisting of flipping spins and moving the spatial occupation while keeping the particle number fixed. If the new state is not already occupied, the move was accepted with probability equal to  $\exp(-\beta(e_{new}(\theta) - e_{old}(\theta)))$ . Fig. 5 shows the convergence of magnetization distribution versus the number of fermions. We found that one could determine the phase transition within a few percent accuracy in the coupling constant  $b$  using only 54 fermions. Such accuracy within PBC would require thousands of fermions because of the strong shell effects.

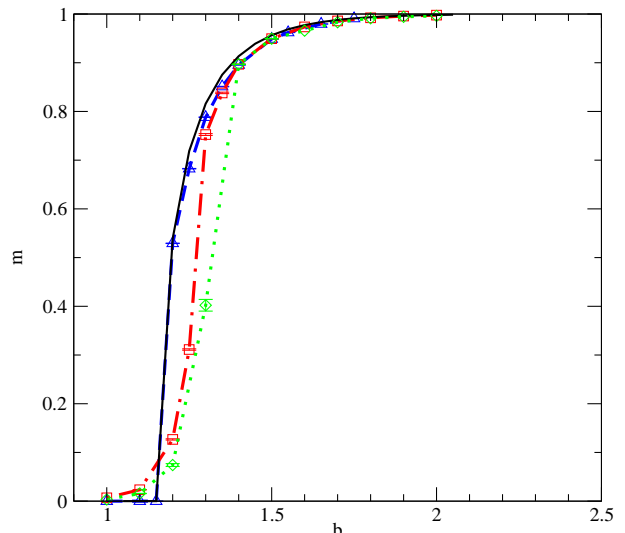


FIG. 5. Magnetization as a function of  $b$  for the 3D Stoner model. Circles are the exact results, diamonds for 54 electrons with PBC, squares for 54 electrons with TABC and triangles for  $N=200$  with TABC. The temperature was  $T = 0.224E_F$  and a  $8^3$  grid of twist values was used.

#### V. ELECTRON GAS

We now present results for the 3-D electron gas as a test of TABC on a correlated many-body continuum system. The electron gas is a very important model

in condensed matter physics being the basis for the density functional theory method of electronic structure computations.<sup>28</sup> The phase diagram of the electron gas at low density is still not resolved<sup>27</sup>. The wavefunctions we use are the most accurate known for a continuum many-body system with optimized 2-body, 3-body and back flow terms. Variational MC (VMC) and Diffusion (DMC) are QMC methods appropriate to zero temperature, and Path Integral (PIMC) to  $T > 0$ . In this paper, we will only discuss VMC and DMC. PIMC will be discussed in future publications.

In VMC, one assumes an analytic form for a trial function  $\Psi_T(R)$  where  $R$  symbolizes the  $3N$  coordinates. Then one samples  $|\Psi_T(R)|^2$  using a random walk<sup>7</sup>. An upper bound estimate to the exact ground state energy is the average of the local energy  $E_L(R) = \Psi_T(R)^{-1} \mathcal{H} \Psi_T(R)$  over the random walk. An accurate trial wavefunction is obtained from the NI wavefunction by multiplying by pair correlation terms. The pair product or Slater-Jastrow wave function is:

$$\Psi_2(R) = \text{Det}(e^{i\mathbf{k}_i \cdot \mathbf{r}_j}) e^{-\sum_{i < j} u(r_{ij})}. \quad (14)$$

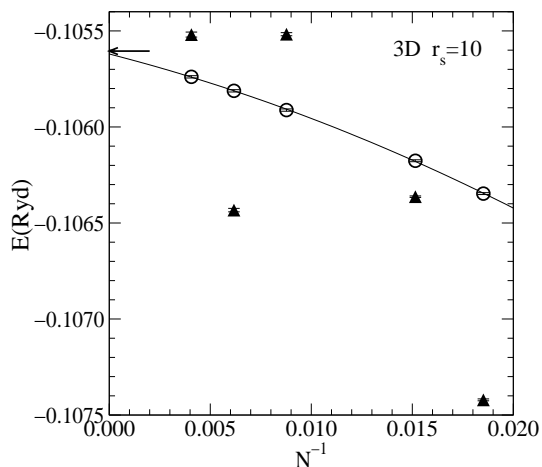


FIG. 6. Energy versus the number of electrons for the 3D electron gas using SJ wavefunction. The circles and connecting line are TABC with  $10^3$  twist values. The filled  $\Delta$ 's are using PBC. The arrow shows the extrapolation to an infinite system made using the PBC calculations using Eq. 16.

One can determine the correlation factor  $u(r)$  either with an analytic argument or by a minimizing of the energy and/or the variance of an assumed form. We use a parameter-free analytic form so that the systematic size and twist effects are not masked by noise in the trial function itself. For the electron gas very accurate analytic form for  $u(r)$  based on the energy within the RPA approximation<sup>29</sup> has as low an energy as those with optimized parameters. We used optimized Ewald sums<sup>30</sup> both for the potential and for the correlation factor so as to have the correct long wavelength behavior.

Fig. 6 shows the convergence of the VMC energy versus the number of particles within TABC and PBC. One can see the convergence to the thermodynamic limit that was found within the NI system is also evident within VMC using the SJ wavefunction. In addition to the Slater-Jastrow trial functions, we also have used optimized backflow-three body functions(BF3B)<sup>9</sup> which give a more accurate description of the low-density electron gas. (They pick up about 3/4 of the remaining correlation energy<sup>9</sup> and break certain symmetries of the SJ wavefunctions.)

In the Diffusion Monte Carlo (DMC) method, one starts with a trial function and uses  $\exp(-tH)$  to project out the ground state using a branching random walk. Fermi statistics pose a significant problem to the projection method, since exact methods such as transient estimate or release-node QMC suffer an exponential loss of efficiency for large numbers of particles. For this reason the approximate fixed-node method is normally used. Using the fixed-node method, one obtains the best upper bound to the energy consistent with an assumed sign of the wave function. Both the FN method and the exact transient estimate can be generalized to treat complex-valued trial functions.<sup>31</sup> These methods are called the fixed-phase and released phase QMC. We have tried both of these approaches using TABC.<sup>32</sup>

## VI. FERMI LIQUID THEORY AND TABC

Fermi liquid theory (FLT) for metallic systems allows both a method to extrapolate to the thermodynamic limit and a way of understanding the twist dependence of the QMC results. According to Landau, the low-lying excitations of an interacting system are in close relation to those of the NI system.

$$E = E_0 + \int d\mathbf{k} \delta n_{\mathbf{k}} e(\mathbf{k}) + \int d\mathbf{k} d\mathbf{k}' \delta n_{\mathbf{k}} \delta n_{\mathbf{k}'} f(\mathbf{k}, \mathbf{k}') + \dots \quad (15)$$

where  $\delta n_{\mathbf{k}}$  is the deviation of the quasi-particle occupation from the ground state, and  $e(\mathbf{k})$  and  $f(\mathbf{k}, \mathbf{k}')$  are 1 and 2 quasiparticle energy functionals. For simplicity we have not indicated dependence on spin. The energy functionals are usually further expanded about the Fermi surface in spherical harmonics and applied to calculate properties in the thermodynamic limit. Here we discuss how to apply FLT when the “excitation” is caused by the boundary conditions. For example, we consider the momentum distribution shown in fig. 1. The change in the energy caused by the non-circular shape should also be given by Eq. 15.

We can analyze this dependence by comparing the energies of the non-interacting system within a given twist with the interacting system. This is done in Fig. 7. One sees a linear relation between the two energies, confirming that for these wavefunctions, Fermi liquid theory is an

appropriate description. The slope is the effective mass of the quasi-particles. Then since the NI infinite energy is known this gives a way of determining the interacting system energy.

Previous calculations on the electron gas have used another application of FLT, the extrapolation method<sup>29,33</sup>. In this method, one calculates accurate ground state energies for a sequence of particle numbers, and determines the effective mass, potential correction and infinite system energy by fitting these energies to the relation:

$$E_N = E_\infty + (m/m^*)\Delta T_N + \epsilon N^{-\nu} \quad (16)$$

where  $\Delta T_N$  is the deviation of the NI kinetic energy from the infinite system and  $\nu$  is the exponent for the potential energy given in Table I. Figure 6 shows that the estimate of the infinite system energy obtained using TABC and the extrapolation method agree within errors. This is reassuring, but expected, since both are based on FLT.

However, applied in practice, there are significant advantages to the TABC method. The fitting method requires well converged runs for at least three different values of  $N$ . This can be difficult, for example when the unit cell is large. For example, suppose one is doing a simulation of bcc hydrogen where one is limited to values of  $N$  equal to  $2K^3 = \{2, 16, 54, 128, 250 \dots\}$ . The last 3 values are reasonable to simulate, however, if the unit cell contained 10 electrons, for example, the extrapolation, would be very difficult without further approximations. There is also the problem that convergence and trial functions for large  $N$  may differ from that for small  $N$ . For example, one typically determines  $m/m^*$  and  $\epsilon$  within VMC and then applies the extrapolation using the DMC energies. There are other problems with extrapolation. For example, suppose we have a partially spin polarized system with say  $n_1$  spin up particles and  $n_2$  down particles. Using PBC there are no necessarily larger, closed shell systems with precisely the same ratio  $\zeta = (n_1 - n_2)/(n_1 + n_2)$ .

Within TABC, there is the possibility of obtaining results in the thermodynamic limit, using only quantities computed for a single value of  $N$ . Figures 7-8 demonstrate that the kinetic contribution is well controlled. Other methods<sup>34</sup> are needed to make the potential correction also for a fixed  $N$ . Use of TABC should make this more accurate as well, as demonstrated in fig. 4.

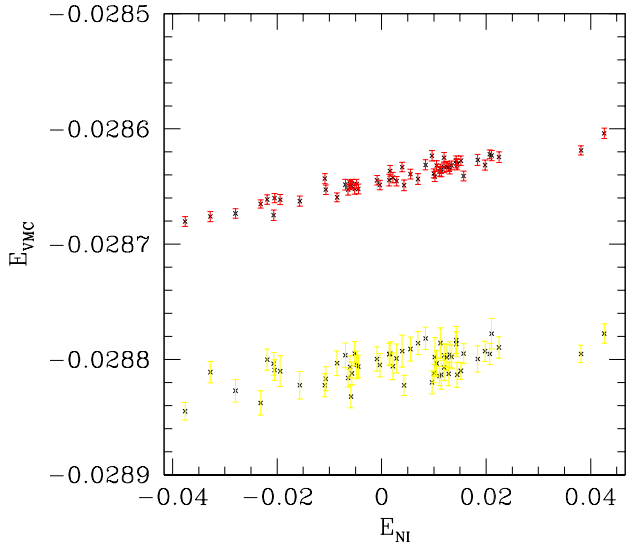


FIG. 7. Plot of the VMC energy versus the deviation of the NI energy from  $E_\infty$ . Each phase angle is plotted separately. Simulations are for  $N = 54$  unpolarized 3D electron gas at  $r_s = 50$ . Since the excitations are linearly related, Fermi liquid theory describes the phase angle dependence. Upper points are the Slater-Jastrow wavefunction, lower ones are done with the backflow-3-body trial function. Effective masses (the slope) are respectively 1 and 0.61 for the two trial functions.

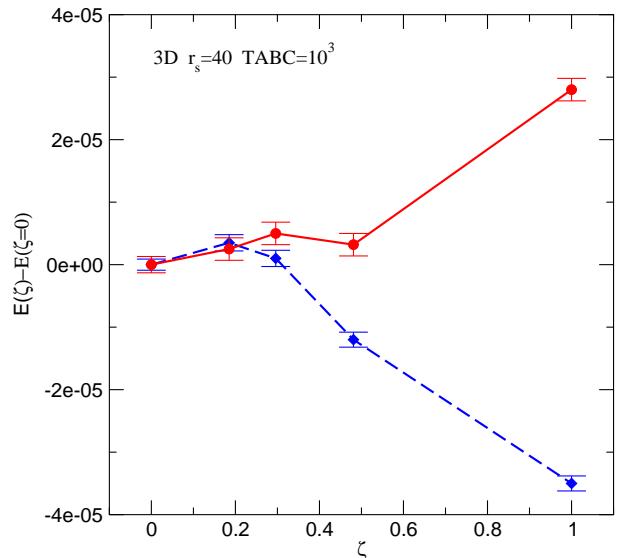


FIG. 8. Energy versus spin polarization for the 3D electron gas at  $r_s=40$  and  $N = 54$ . The dashed line is with the Slater-Jastrow function, the solid line with backflow-3-body trial function. Calculations are done using VMC with  $10^3$  twist values.



## VII. OTHER PROCEDURES USING TWISTED BOUNDARY CONDITIONS

**Dynamical twist method.** As an alternative to TABC, one can let the twist angle be a dynamical variable (DTBC) and be determined self consistently. By dynamical is meant that the probability of a given twist is proportional to its free energy:

$$P(\theta) \propto \exp(-\beta F(\theta)) = \sum_{\alpha} \exp(-\beta E_{\alpha}(\theta)) \quad (17)$$

where  $E_{\alpha}(\theta)$  is the energy of the state  $\alpha$  with twist  $\theta$ . This distribution of twist angles could be attained within QMC by enforcing detailed balance on moves of the twist angle during a random walk. The expectation of an operator  $A$  will be:

$$\langle A \rangle_{DTBC} = \frac{1}{Z} \int d\theta e^{-\beta F(\theta)} \langle \Psi_{\alpha}(\theta) | A(\theta) | \Psi_{\alpha}(\theta) \rangle. \quad (18)$$

At zero temperature, a special set of twist angles, those which have the lowest energy, will be singled out, so that the ground state energy will be  $E_{DTBC} = \min_{\theta}(E(\theta))$ . Clearly  $E_{DTBC} \leq E_{\infty}$ , in contrast to the TABC which gives an upper bound. In general, the dynamical energy,  $E_{DT}$  converges as slowly to the thermodynamic limit as does the PBC energy: the exponents and fluctuations are the same. The dynamical twist method is not an improvement over PBC for approaching the thermodynamic limit for a metallic system at temperatures much lower than the fermi temperatures.

Although the dynamic twist method is not satisfactory for a Fermi liquid at low temperatures, for certain lattice models such as an antiferromagnetic Heisenberg model, it can be a definite improvement over PBC and TABC. This is because one can only establish a defect-free Néel ordering if the unit cell is commensurate with the boundary conditions. For the Heisenberg model on a triangular lattice, the ground state has a given twist per lattice spacing. Using DTBC allows one to establish this twist value automatically, without imposing it in advance. This is equivalent to the classical variable cell method where the dimensions and aspect ratio of the supercell of a crystal become dynamical variables, so that one can determine the most stable crystal lattice structure<sup>35</sup> instead of examining each crystal structure explicitly.

**Special points** For each value of  $N$  there exists a set of twist values for which  $E(\theta) = E_{\infty}$ . One can determine these special twist values for the NI system and then perform simulations at only one of those twist values for the interacting system, thereby getting rid of single particle size effects. This is similar to the special k-point method of Baldereschi<sup>11</sup> for insulators where a single k-point is determined by symmetry, thus allowing one to replace an integral over the Brillouin zone with evaluation at a single k-point. This method was used within QMC by Rajagopal et al.<sup>17</sup>.

The special k-point method is not appropriate for a metal because of the discontinuity in properties at certain twist values. One cannot replace the average by a single point because the Fermi surface is not given in advance by symmetry, and can change between the interacting and non-interacting wave functions. In addition, it is not expected that the same twist values appropriate for the NI energy, will be appropriate for other quantities such as the potential energy, or spin susceptibility. It is better to have a method which can give a spectrum of properties correctly, rather than only the kinetic energy. As we discuss in the Appendix, TABC does not impose an excessive computational burden, and is to be preferred over using only special twist values.

## VIII. CONCLUSIONS

Note that there is a significant difference in the efficiency for stochastic (QMC) methods versus explicit methods such as density functional theory or exact diagonalization in regards to the TABC. In explicit methods, computations for each twist require an equal amount of computer time so that averaging over  $N_G$  twist values will take roughly  $N_G$  times as long as a single twist value. One can use inversion and rotational symmetry to reduce this, so that for a grid of  $16^3$  points, TABC will require only 165 twists. On the other hand, in QMC all the twists reduce the statistical error of the average. The twists are simply three more degrees of freedom on top of the  $3N$  coordinate variables to be averaged over. However, one must also take into account startup costs associated with each twist, such as re-optimizing the trial wavefunction or equilibrating the random walk. Neglecting these startup costs, there is no loss of statistical efficiency in performing TABC so that the gain in reducing the systematic error is free. This is examined in more detail in the Appendix.

There are many examples where twist averaging can effect considerable improvement over the use of PBC. We have been able to perform quite accurate calculations of the polarization energy of the 2 and 3D electron gas<sup>32</sup> and of liquid <sup>3</sup>He using backflow wavefunctions with on the order of 100 fermions. As pointed out by Ortiz et al.<sup>27</sup> calculations on such small systems in PBC have considerable systematic errors. One property that could be computed more accurately with TABC is the estimation of fermi liquid parameters by calculating particle-hole excitation<sup>36</sup>. TABC can reduce the shell effects which caused much difficulty in that calculation. A related example is in computation of the charge response of the electron gas<sup>37</sup> where a considerable effort was made to cancel out effects of the PBC. We are presently studying the electron gas confined to a slab<sup>38</sup> to determine the work function and surface energy of a metallic surface. The filled states consist of a set of disks, each of which will have a certain occupation number. By doing twist

averaging we have shown reduced size effects with respect to PBC.

Experimental systems are at a non-zero temperature. For NI systems one occupies the states with probability given by the Fermi-Dirac distribution. Because the Fermi function at non-zero temperature is a continuous function, the convergence to the thermodynamic limit will be much faster, even with PBC. However in practice, one is interested in electronic systems close to the ground state; the relevant quantity is the thermal deBroglie wavelength of the electron:  $\hbar/(m_e k_B T)^{1/2} \approx 32\text{\AA}$  at  $T = 300\text{K}$ . Because this length is usually larger than the simulation cell in QMC, the localization of the density matrix does not help at reducing fermion finite size at these temperatures. Using a non-zero temperature just to achieve faster convergence to the thermodynamic limit is not practically useful. However, TABC is extendable to finite temperature PIMC simulations using the fixed-phase method<sup>31</sup> and will reduce size effects at low temperature.

The TABC method is likely to be valuable for all QMC calculations in systems with a fermi surface. The calculations on the electron gas demonstrate that even though it may be a little slower per step of the random walk, it is better to do TABC than a larger system with periodic boundary conditions because TABC converges much faster to the thermodynamic limit. The overall efficiency of any numerical method is ultimately judged by the computer time needed to reduce systematic **and** statistical error below a given value. TABC is effective in reducing the systematic errors and thus improve the overall efficiency.

This research was supported by NSF DMR-98-02373 and the Department of Physics at the University of Illinois Urbana-Champaign. We acknowledge useful discussions with R. M. Martin and G. Bauer. Computational resources were provided by the NCSA. We thank H. Edelsbrunner for references concerning Gauss' circle problem.

## APPENDIX

Here we discuss numerical details of implementing twist averaged boundary conditions. Many of the changes caused by twisted boundary conditions arise from the need to have complex wavefunctions. Although the wavefunction and energies in special cases are real (*e.g.* PBC and ABC), complex functions are needed for general twist angles. There is a factor of roughly 2.5 in additional CPU time to do the arithmetic to evaluate the determinant and its derivatives. The actual impact on the total speed is smaller than this because the calculations of two-particle quantities such as the potential energy and correlation factors are still done with real arithmetic; the actual penalty of working with non-zero twist depends on the number of particles and the type of the trial wavefunction. However, as we have discussed

earlier, even a factor of 2.5 in computer time is worthwhile if one is able to approach the thermodynamic limit quicker, since QMC methods scale as  $N^\nu$  with  $1 \leq \nu \leq 4$  or, in the case of exact fermion methods, as  $\exp(\gamma N)$ . If TABC saves going to larger  $N$ , the additional time doing complex arithmetic is well justified.

There are several alternatives for performing the twist averaging:

1. Evaluate as  $\sum_i w_i E_i$  using a grid defined by points  $\theta_i$  with weights  $w_i$  (with  $\sum_i w_i = 1$ ) in the region specified by Eq. 2.
2. Sample the twist during the QMC random walk and take the average.
3. A combination of the two approaches: working on a grid that is augmented with random displacements.

As we discuss below, all three methods are satisfactory; there is no fundamental difference in efficiency. The choice of whether to sample or use a grid is primarily based on convenience and programming considerations and only secondly on efficiency. We note that all methods are easy to parallelize.

**Grid averaging.** First, we must address the question of which grid and integration rule to use. Since all properties are periodic with respect to the twist, the grid should be a Bravais lattice with equally weighted points. One must keep in mind that the properties, though periodic and continuous, have discontinuous derivatives at the Bragg planes. Unless grid points can be located on these planes (which is difficult to achieve in practice), the integration error will go as  $\epsilon_G \propto \Delta\theta^2 \propto N_G^{-2/D}$  where  $N_G$  is the number of grid points. Numerically, we find that  $16^3$  grids are needed for an accuracy of  $10^{-3}$  (see table I). This slowly convergent, systematic error is the main drawback of the grid integration method. For an insulator with a large enough gap to excitations, properties would be analytic for all  $\theta$  since the occupation of single particle states will not change as a function of twist angle and the grid error would converge exponentially fast.

Once a grid is chosen, one can use symmetry (*e.g.* inversion and rotation through  $90^\circ$ ) to reduce the number of grid points and give them a weight ( $w_i$  with  $\sum_{i=1}^{N_G} w_i = 1$ ) proportional to their multiplicity. It is easy to show that the optimal amount of computer time at each grid point should be chosen proportional to  $w_i/\zeta(\theta_i)^{1/2}$  where the MC efficiency at  $\theta_i$  is defined as  $\zeta(\theta_i) = 1/(\text{var}(E(\theta_i))\text{cputime})$ . We have found on the calculations of the electron gas described earlier, that this efficiency is independent of the twist angle except at the special PBC and ABC points where real functions can be used. Even though we have symmetry and can integrate over a reduced set of twist values, we must integrate longer at high multiplicity points since they contribute more to the average. Hence, the symmetry does not significantly reduce the needed amount of CPU time.

Since the calculations at different twist angles are uncorrelated, one can easily show that the efficiency of calculating the twist averaged energy is given by the relation:

$$\zeta^{-1/2} = \sum_{i=1}^{N_G} w_i \zeta^{-1/2}(\theta_i). \quad (19)$$

Hence, the overall efficiency of the TABC energy is an average of the efficiencies of the individual twist calculations and is higher than that of the slowest converging twist angle. The additional averaging over twist angle costs nothing in efficiency.

However, this discussion did not take into consideration start-up costs at each twist angle, such as the need to reoptimize the trial wave function at a new twist value, and equilibration costs. By equilibration, we mean that whenever the twist angle is changed, enough random walk steps must be taken so that the configurations are sampled from the new twist value. During this equilibration, averages cannot be taken. These computational costs cause a decrease of efficiency by the factor (useful time)/(total time) and are the main extra computational penalty of the TABC method within QMC. Since the startup time will scale with the number of needed grid points, using the above estimate of the systematic error,  $\epsilon_G$ , we find that the needed startup time scales as  $\epsilon_G^{-d/2}$  while the time to achieve equivalent statistical error scales as  $\epsilon^{-2}$ . Hence, for very precise calculations ( $\epsilon \rightarrow 0$ ) and  $d < 4$ , startup costs can be neglected.

**Twist sampling.** Now consider the second alternative, where the twist angle is sampled during the random walk. With this method, we do not have to decide on a grid in advance and there is no systematic error of a finite grid.

Again, one must equilibrate the configurations after the change of twist angle and computer time used in that process does not reduce the variance of the average.

There is an additional increase in variance caused by sampling the twist angle. One can show that the efficiency decreases by a factor:  $[1 + E_{BW}^2 / \text{var}(E_\theta)]^{-1}$  where  $E_{BW}$  is the “band-width” defined in Eq. 5. If one spends too long at a given twist angle, one is not adequately exploring the twist angle degree of freedom. This gives a definite rule for how often the twist angle should be updated: the time spent at a given twist angle should be much longer than the equilibration time but less than the time needed to get the error in the energy at that twist value equal to the “bandwidth” of the system. If it is not possible to achieve this relation, the grid scheme should be used.

With either method, one can achieve more accurate results and less systematic error by correcting the results using Fermi liquid theory. That is, using the twist values and corresponding energies one can estimate the effective mass and twist averaged energy using a least squares fit as discussed in Section VI. However, there could be additional statistical and systematic error resulting from the fit.

Finally, one can combine the positive features of two methods using antithetic sampling: use a relatively coarse grid, but then randomly displace the origin of the grid a number of times during the run, so as to eliminate the systematic error of the grid and estimate the true errors. Since the twist angle will change by a small amount, setup time and equilibration time can be reduced. A related approach is to sample the twist angle using a quasi-random number sequence so as to reduce the dispersion of the twist values.

---

<sup>1</sup> We follow the usage of others in calling  $\theta$  the *twist angle* rather than the phase angle to avoid confusion with all the other usages of the word phase that appear in quantum and statistical physics.

<sup>2</sup> A. J. Leggett, *Physica Fennica*, **8**, 125 (1973).

<sup>3</sup> N. Byers and C. N. Yang, *Phys. Rev. Letts.* **7**, 46 (1961).

<sup>4</sup> Note also that all identical particles must have the same twist.

<sup>5</sup> This technique has also been called Integration over Boundary Conditions (IBC)<sup>16</sup> and Phase Randomization<sup>15</sup>.

<sup>6</sup> D. Poilblanc, *Phys. Rev. B* **44** 9562(1991).

<sup>7</sup> D. M. Ceperley, G. V. Chester and M. H. Kalos, *Phys. Rev. B* **16**, 3081 (1977).

<sup>8</sup> Y. Kwon, D. M. Ceperley and R. M. Martin, *Phys. Rev. B* **48**, 12037 (1993).

<sup>9</sup> Y. Kwon, D. M. Ceperley and R. M. Martin, *Phys. Rev. B* **58**, 6800 (1998).

<sup>10</sup> D. Ceperley and B. J. Alder, *J. Chem. Phys.* **81**, 5833 (1984).

<sup>11</sup> A. Baldereschi, *Phys. Rev. B* **7**, 5212 (1973).

<sup>12</sup> H. J. Monkhorst and J. D. Pack, *Phys. Rev. B* **13**, 5188 (1976).

<sup>13</sup> I. Souza, T. Wilkens and R. M. Martin, *Phys. Rev. B* **62**, 1666 (2000).

<sup>14</sup> R. Julien and R. M. Martin, *Phys. Rev. B*, **26**, 6173 (1982).

<sup>15</sup> E. Y. Loh, Jr. and D. K. Campbell *Synthetic Metals* **27** A499 (1988); J. Tinka Gammel, D. K. Campbell, and E. Y. Loh, Jr., *Synthetic Metals* **55-57**, 4437 (1993).

<sup>16</sup> C. Gros, *Z. Phys. B* **86**, 359 (1992); *Phys. Rev. B* **53**, 6865 (1996); R. Valenti, C. Gros, P. J. Hirschfeld and W. Stephan, *Phys. Rev. B* **44**, 13203 (1991).

<sup>17</sup> G. Rajagopal, R. J. Needs, S. Kenny, W. M. C. Foulkes and A. James, *Phys. Rev. Letts.* **73**, 1959; *Phys. Rev. B* **51**, 10591 (1995); *Phys. Rev. B* **51**, 10591 (1995).

<sup>18</sup> B. Krlik, P. Delaney, and S. G. Louie, *Phys. Rev. Letts.* **80**, 4253 (1998).

<sup>19</sup> C. Filippi and D. M. Ceperley, *Phys. Rev. B* **59**, 7907 (1999).

<sup>20</sup> N. W. Ashcroft and N. D. Mermin *Solid State Physics*, pg.

- 162, Saunders Co. The bisecting plane between the origin and any reciprocal lattice vector of the Bravais lattice are Bragg planes. The  $n^{\text{th}}$  Brillouin zone is the set of points that can be reached from the origin by crossing exactly (n-1) Bragg planes.
- <sup>21</sup> Encyclopedic Dictionary of Mathematics, ed. S. Iyanaga and Y. Kawada, MIT press 1980, pg. 749.
- <sup>22</sup> D. G. Kendall, Quart. J. Math. (Oxford), **19**, 1 (1948).
- <sup>23</sup> E. Stoner, Proc. Roy. Soc. A **165**, 372 (1939); A **169**, 339 (1939).
- <sup>24</sup> R. A. Suris, Sov. Phys, Solid State **3**, 1303 (1961).
- <sup>25</sup> C. Herring, in *Magnetism*, vol **IV**, (eds. G. T. Rado and H. Suhl) (Academic Press, San Diego, 1966).
- <sup>26</sup> B. J. Alder, D. M. Ceperley and E. L. Pollock, Int. J. of Qu. Chem. **16**, 49 (1982).
- <sup>27</sup> G. Ortiz, M. Harris and P. Ballone, Phys. Rev. Letts. **82**, 5317 (1999).
- <sup>28</sup> D. M. Ceperley and B. J. Alder, Phys. Rev. Letts. **45**, 566 (1980).
- <sup>29</sup> D. M. Ceperley, Phys. Rev. B **18** 3126, (1978).
- <sup>30</sup> V. Natoli, D. and Ceperley D. M., J. Comput. Physics **117**, 171 (1995).
- <sup>31</sup> G. Ortiz, D. M. Ceperley and R. M. Martin, Phys. Rev. Letts. **71**, 2777 (1993).
- <sup>32</sup> C. Lin, PhD thesis, University of Illinois Urbana-Champaign, 2000.
- <sup>33</sup> D. M. Ceperley and B. J. Alder, Phys. Rev. B **36**, 2092 (1987).
- <sup>34</sup> P. R. C. Kent, R. Q. Hood, A. J. Williamson, R. J. Needs, W. M. C. Foulkes and G. Rajagopal, Phys. Rev. B **59**, 1917 (1999).
- <sup>35</sup> M. Parrinello and A. Rahman, Phys. Rev. Letts. **45**, 1196 (1980).
- <sup>36</sup> Y. Kwon, D. M. Ceperley, and R. M. Martin, Phys. Rev. B **50**, 1684 (1994).
- <sup>37</sup> S. Moroni, D. M. Ceperley and G. Senatore, Phys. Rev. Lett. **75**, 689 (1995); pgs. 183-212 in *Quantum Monte Carlo Methods in Physics and Chemistry*, eds. M. P. Nightingale and C. J. Umrigar, Kluwer, 1999.
- <sup>38</sup> X. P. Li, R. J. Needs, R. M. Martin and D. M. Ceperley, Phys. Rev. B **45**, 6124 (1992).